Published in final edited form as:

Biomater Sci. 2019 May 28; 7(6): 2326–2334. doi:10.1039/c9bm00020h.

Air-plasma treatment promotes bone-like nano-hydroxylapatite formation on protein films for enhanced in vivo osteogenesis

Qing Zhang[†,a,b], **Lu Ma**[†,b], **Shengnan Zheng**[b], **Yaru Wang**[a], **Meilin Feng**[a], **Yajun Shuai**[a,b,c], **Bo Duan**[a], **Xin Fan**[a], **Mingying Yang**[a], and **Chuanbin Mao**[b,c]

[a.] Institute of Applied Bioresource Research college of Animal Science, Zhejiang University, Yuhangtang Road 866, Hangzhou 310058, China.

[b.] School of Materials Science and Engineering, Zhejiang University, Hangzhou 310027, China

[c.] Department of Chemistry & Biochemistry Stephenson Life Sciences Research Center Institute for Biomedical Engineering, Science and Technology University of Oklahoma 101 Stephenson Parkway, Norman, Ok 73019-5300, USA.

Abstract

Introducing hydroxylapatite (HAp) into biomolecular materials is a promising approach to improve their bone regnerative capability. Thus a facile method needs to be developed to achieve this goal. Here we show that a simple air-plasma treatment of silk fibroin (SF) films for 5 min induced the formation of bone-like plate-shaped nano-HAp (nHAp) on their surface and the resultant material efficiently enhanced in vivo osteogenesis. The air-plasma-treated SF films (termed A-SF) presented surface nano-pillars and enhanced hydrophilicity compared to the pristine SF films (termed SF), making the A-SF and SF films induce the formation of plate-shaped/more-crystalline and needle-like/less-crystalline nHAp, respectively. The mineralized A-SF and SF films (termed A-SF-nHAp and SF-nHAp, respectively) and their non-mineralized counterparts were seeded with rat mesenchymal stem cells and subcutaneously implanted into the rat models. The A-SF-nHAp and A-SF films exhibited more efficient bone formation than the SF-nHAp and SF films in 4 weeks due to their unique nanotopography, with the A-SF-nHAp films being more efficient than the A-SF films. This work shows that a combination of the air-plasma treatment and the subsequent nHAp mineralization most efficiently promotes bone formation. Our plasma-based method is an attractive approach to enhance the bone regenerative capacity of protein-based biomaterials.

Introduction

Biomacromolecules, such as collagen, chitosan and polycaprolactone, are applied as templates to induce the biomineralization and assembly of hydroxylapatite (HAp) and prepare composite scaffolds as bone implants.[1–3] Besides, most of them exhibited good

yangm@zju.edu.cn, cbmao@ou.edu.

[†]These authors contributed equally to this work.

Conflicts of interest

There are no conflicts to declare.

bone-like tissue regenerative ability. Compared with these polymers, silk fibroin (SF) can be easily produced and exhibit desired mechanical and functional properties for biomedical applications because of its low immunogenicity, oxygen and water vapor permeability, good biocompatibility and superior mechanical properties.[4] Earlier we reported that *B.mori* SF powders could mediate HAp mineralization through the SF self-assembly in a co-solution of 1.5 simulated body fluid (SBF) and SF molecules.[5] The negatively charged -COOH groups in the acidic amino acids (e.g., Asp and Glu) in another silk-derived protein, *B.mori* sericin, could bind positively charged Ca^{2+} in a mineralization solution buffer, which triggered the nucleation of HAp.[6] However, nano-HAp (nHAp) with a tunable morphology regulated by a SF matrix has not been reported.

On the other hand, various SF scaffolds were mineralized with nHAp to prepare SF/nHAp composite scaffolds. They showed excellent biocompatibility, osteoconductivity and osteoinduction, and have been widely investigated in repairment and reconstruction of bone tissue.[7, 8] The osteoinduction of SF/nHAp scaffolds was attributed to the interaction between the scaffolds and cells, and such interaction was associated with the assembly, crystalline degree, shape and size of nHAp.[9, 10] However, as far as we know, no studies have been done to demonstrate the relationship between osteoinduction of SF/nHAp scaffolds and the morphology of nHAp on their surface. This is probably because SF/nHAp composite scaffolds with tunable morphology of nHAp on the surface have not been developed. To fill this gap, in this work we formed SF films coated with nHAp of two different shapes (plate-like and needle-like) and then studied the *in vivo* osteogenesis directed by the resultant SF/nHAp composites.

The surface properties of SF films can influence the mineralization and aggregation of nHAp on them. Chemical or physical processes are often used to improve the SF materials surface properties.[11–13] In general, chemical processes usually use genotoxic or cytotoxic chemical reagents (such as glutaraldehyde),[14] which might result in modified films with undesired cytotoxicity, and thus are not desired in modifying SF films. Plasma treatment, as a physical process without the need of water and chemicals, is a more economical, secure and ecological process than the wet chemical process.[15, 16] Besides, plasma treatment will not change inherent properties of natural polymers. Hence, low temperature plasma treatment is a promising process for improving the surface properties of natural polymer matrix, for instance, shrinking resistence, wetting, anti-bacterial property, hydrophilicity and hydrophobicity.[17–20] As a relatively cheap and readily available gas, air was an ideal source to generate low temperature plasma for treating the SF. Therefore, in this study, we used air plasma to modify the surface of pristine SF films (termed SF) and then employed the air-plasma-treated SF films (termed A-SF) to template the mineralization of nHAp with a bone-like plate-shaped morphology, generating a composite film termed A-SF-nHAp. In contrast, the pristine SF films only induced the formatin of needle-like nHAp on the surface to form a mineralized composite termed SF-nHAp. We found that the A-SF-nHAp films could more efficiently induce the bone formation *in vivo* in a rat subcutaneous model than the A-SF films, which were also found to be more efficient in inducing bone formation than both the pristine SF films and SF-nHAp films (Fig. 1).

Experimental Section

Preparation of SF films

B. mori silkworm cocoon were used to produce the aqueous SF solution through our prevously described procedures.[21] The prepared SF solution was concentrated by the solvent evaporation method in the dialysis membrane. To prepare a SF film (2 mm thick), 3 ml of 8% (w/w) SF aqueous solution was casted onto a plastic culture plate with 5 cm diameter, followed by air drying at room temperature. Prior to mineralization, the SF film was immersed in 70 % (v/v) methanol in order to turn the secondary structure of the SF molecules into a β-folding structure.

Air plasma treatment of SF

The SF was put into the vacuum chamber of a plasma cleaner (YZD08–2C, Beijing boya innovation technology development co. LTD, China). Air was leaked into the plasma cleaner to reach 100 Pa. A 100 W radio frequency power was applied to initiate the plasama treatment of the SF film for 5 min. The resultant plasma-treated SF was termed A-SF.

Mineralization of nHAp on the SF and A-SF films

The mineralizaiton of nHAp was performed by immersing the SF or A-SF films in a liquid-solid-solution, which was used for the synthesis of HAp nanorods invented by Li et al.[22] In short, 16 ml ethanol, 4 ml linoleic acid and 0.5 g octadecylamine were mixed together under stirring. Following this step, 7.5 ml 0.4 M $Ca(NO_3)_2$ aqueous solution was added into the mixture. 10 min later, 7.5 ml 0.4 M Na_3PO_4 solution was placed into the mixture under agitating for 5 min. The SF or A-SF films were put into the final mixture solution to realize the nHAp mineralization on them. The SF and A-SF films with mineralized nHAp were termed SF-nHAp and A-SF-nHAp, respectively.

Structural and morphological characterization of various films

The surface morphologies of the films were visualized by scanning electron microscope (SEM, SU8010, Hitachi Limited). Samples were coated with platinum by using an ion-sputter coater prior to the imaging. X-ray diffraction (XRD, X-pert Powder, PANalytical) and Fourier transform infrared (FT-IR, FITR-8400, SHIMADZU) spectroscopy were applied to analyse the phase composition and chemical structures of the films, respectively. To carry out XRD analysis, the samples were grinded into powders, which were scanned from 0 ~ 90°with a scanning rate of 5°/ min at 40 kV. To perform FTIR analysis, all samples were cut into fragments and pressed into transparent films with KBr (1% w/w). All FTIR measurements were done with 120 scans and a resolution of 4 cm^{-1}. The FTIR spectra were generated within the spectral range of 4000–400 cm^{-1} in the transmittance mode. The chemical compositions of the surface of the films were revealed by X-ray photoelectron spectroscopy (XPS, Escalab 250Xi, Termofisher) using Mg Kα line (1253.6 eV) with a passing energy of 11 eV. The hydrophilic-hydrophobic property of various films was determined by measuring the static contact angles at room temperature and 60% relative humidity. Three regions were measured for each sample of SF, A-SF, SF-nHAp and A-SF-

nHAp films. The measurements were conducted using a contact angle meter (DCA20, Dataphysics).

The culturing and seeding of MSCs on various films

Bone marrow derived MSCs of SD rat, bought from Cyagen Biosciences, were cultured in a low glucose Dulbecco's modified Eagle medium (DMEM) containing 1 % penicillin/streptomycin antibiotics and 10% fetal bovine serum (FBS) at 37 °C in an incubator. MSCs at the sixth passage were utilized in this study. To seed MSCs on the films, all films were first cut into small round pieces and put into culture plates. After the films in the plates were sterilized with 75 % (v/v) ethanol, remnent ethanol was wiped off by washing the plates with phosphate buffered solution (PBS). MSCs (4×10^4 cell/well) were then seeded onto the SF, A-SF, SF-nHAp and A-SF-nHAp films.

Morphology of MSCs on resultant films

After being seeded on the films for 1 and 3 days, MSCs were fixed with a 4 % paraformaldehyde solution for 30 min, followed by the penetration of 0.1 % Triton X-100. The actin of MSCs was then stained with phalloidin-iFluorTM 488 Conjugate (23115, AAT Bioquest, USA). The cell nuclei were stained with DAPI (C1002, Beyotime, China). Then a confocal laser scanning microscope (CLSM) was applied to observe the morphology of MSCs on the films.

MSCs viability assay on films

The viability of the MSCs on the different films was tested by CellTiter 96® AQueous One Solution Cell Proliferation Assay (promega, USA). In brief, after being cultured for different times, the MSCs were incubated with 200 μl work reagent for 1 h. Then a microplate reader was used to read the absorbance at 490 nm. Each group included four samples for each time point.

Evaluation of osteogenesis *in vivo*

An SD rat subcutaneous model was built using a reported method.[23] SD rats (~200 g each) were subject to anesthesia using 4 % isoflurane/oxygen. The anesthesia was maintained with 2 % isoflurane during the surgical operation. MSC-seeded films with similar shape and size were subcutaneously implanted into the back of SD rats. When the incision was closed, a 2 % lidocaine solution was immediately injected to the surgical area at the 1 ml/kg dosage. Subsequently, each rat was intramuscularly injected with penicilin for four consecutive days. After 4 weeks of implantation, implanted films were taken out of the rats and fixed with 10 % neutral formalin. The films were then processed, embedded with paraffin and sectioned. Then 5 μm thick sections of each sample were used for histological and immunohistochemistry analysis. Hematoxylin and eosin (H&E) staining was applied for histological analysis. Immunohistochemical staining of bone matrix proteins, including collagen I (Col- I), osteocalcin (OCN) and osteopontin (OPN), were used to visualize the bone tissue formation around the films. Briefly, the sections were incubated first in a H_2O_2 solution and then in normal serum to block endogenous peroxidase activity and unspecific staining. Then the sections were interacted with a primary antibody (Abcam (ab34710) for

Col- I, Abcam (ab8448) OPN and Abcam (ab13420) OCN) for 1.5 h. Then an HRP-conjugated secondary antibody was applied to treate the rinsed sections. Last, the staining intensity was realized through an appropriate 3,3'-diaminobenzidine solution. All stained sections were photographed by a light microscope. The semi-quantitative analysis of the expression levels of Col- I, OPN and OCN was performed using Image J software. The average optical density (AOD) for each sample was obtained from at least three fields. All procedures of the *in vivo* studies were carried out in accordance with the Guidelines for Care and Use of Laboratory Animals of Zhejiang University and Experiments were approved by the Animal Ethics Committee of Zhejiang University.

Statistical analysis

Data were expressed as mean values ± standard deviation (SD). A two tailed, unpaired student's test was used to evaluate the significance among experiment groups.

Results

The surface morphologies of the films

The morphologies of the surfaces of the SF, A-SF, SF-nHAp and A-SF-nHAp films (Fig. 2) were revealed by SEM. The surface of the pristine SF films was smooth, but nano-pillars were distributed uniformly on the A-SF films (Fig. 2A, a, B and b), making the A-SF surface rougher than the SF surface. The surfaces of the two mineralized films, SF-nHAp and A-SF-nHAp, were covered with needle-like and plate-shaped nHAp, respectively (Fig. 2C, c, D and d).

The contact angles of the films

The hydrophilic-hydrophobic property of the films was characterized by water static contact angles. The static contact angles of SF and A-SF were about 84°and 26°, respectively (Fig. 3a–b). This result indicated that the water wettability of the SF films was improved due to the air-plasma modification. The water static contact angles of SF-nHAp and A-SF-nHAp were about 85° and 84°, respectively (Fig. 3c–d), indicating the nHAp made the films bear similar wettability. Namely, after being mineralized, the films prestented a similar hydrophilic-to-hydrophobic property.

The phase compsitions and chemical structures of the films analyzed by XRD, FT-IR and XPS

FT-IR analysis was performed to study the variation of chemical structures of SF films after different treatments (Fig. 4A). The broad band located at 3291 cm^{-1} was ascribed to stretching vibration of hydroxyl groups and water molecule.[24] The absorption bands at 2869 cm^{-1} and 2973 cm^{-1} corresponded to the symmetric and asymmetric stretching vibration of CH_3 present in the SF molecules.[24] The peaks at 1627, 1524 and 1232 cm^{-1} displayed in Fig. 4A were assigned to amide I, II and III of β-sheets in the SF molecules.[5] The β-sheets in the SF and A-SF films resulted from the impact of methanol solution used during the SF film preparation. The methanol is known to induce the conversion of the secondary structure of the SF molecules from the α-helix and random coil into the β-sheet form. Peaks near 995 cm^{-1} belonged to glycine-alanine-glycine linkage.[25] The absorption peaks at the same

locations were found in the FT-IR spectra of both the A-SF and SF films but presented a lower intensity in the A-SF films than in the SF films, indicating that the air-plasma treatment might break the amide and β-sheet structure of the SF molecules. The two mineralized films (Fig. 4(A–c) and (A–d)) were almost identical in FT-IR spectra. In addition to the absorption peaks for the SF molecules, the mineralized films exhibited two new peaks centered at 1100 cm^{-1} and positioned at 560 cm^{-1}, which were attributed to the υ_3 vibration of the PO_4^{3-} bond and the υ_4 vibration of the PO_4^{3-} bond, respectively.[5] This observation verified the deposition of nHAp on the surface of the SF-nHAp and A-SF-nHAp films.

XRD analysis was employed to investigate the phase compositions of the SF, A-SF, SF-nHAp and A-SF-nHAp films (Fig. 4B). The peaks at 9.0°, 20.5° and 24.7° were found in the XRD patterns of both the SF and A-SF films and they were the specific peaks of silk- II structure in the SF matrix (Fig. 4B).[24] These peaks were broad and weak, suggesting that the SF matrix had a low crystallinity and included random coils. The peak at 12.2°in the XRD pattern of the A-SF films indicated that the content of random coils was increased. The XRD patterns of the two mineralized films (Fig. 4B(c–d)) showed that in addition to the broad peaks at 9° and 24.7° of the underlying SF matrix, new peaks at 25.9°, 32° and 39.7° emerged. These new peaks were the specific crystal diffraction peaks of HAp (JCPDS09–0432)[26, 27], proving the presence of nHAp on the SF-nHAp and A-SF-nHAp films. A closer look at the XRD patterns indicated that more distinct peaks of nHAp were present on the A-SF-nHAp films than on the SF-nHAp films, suggesting that nHAp on the surface of A-SF-nHAp films presented a higher crystallinity than that on the surface of the SF-nHAp films.

The chemical analysis of the various films was realized by using XPS analysis. XPS spectras of the SF and A-SF films (Fig. 4C(a) and (b)) exihibited three stong peaks located at 290, 400 and 530 eV, which could be assigned to C1s, N1s and O1s, respectively.[18] These results suggested that the oxygen content was increased after the air plasma treatment, consistent with the finding that plasma treatment resulted in increase in water wettability of the A-SF films. Besides, the SF-nHAp and A-SF-nHAp films presented the photoelectron peaks located at 134, 190 and 347 eV in the XPS spectra (Fig. 4C(c) and (d)), which were corresponding to P 2p, P 2s and Ca 2p spectra of HAp, respectively. The peaks at 285, 400 and 532 eV corresponded to C 1s, N 1s and O 1s spectra of the SF molecules, respectively.[28, 29]

MSCs viability and morphology on various films

The morphologies of MSCs on the SF, A-SF, SF-nHAp and A-SF-nHAp films after being cultured for 1 day and 3 days were characterized by confocal microscopy via F-actin and nucleus staining, as shown in Fig. 5(A) and (B). The morphologies of MSCs presented no obvious difference on the vrious substrates on day 1. Nevertheless, the MSCs stretched out less pseudopods on pristine SF films than the other three films on day 3. More MSCs were observed on the SF-nHAp and A-SF films than on the A-SF-nHAp and SF films on day 3, consistent with the result of viability assay (Fig. 5C). Moreover, after being seeded for 7 days, MSCs exhibited a stronger proliferation ability on the mineralized or non-mineralized A-SF films than on the mineralized or non-mineralized SF films (Fig. 5C).

Biocompatibility of various films *in vivo*

HE staining was applied to investigate the biocompatibility of the four films (Fig. 6). After being implanted in the subcutaneous rat model for 1 month, all the films did not exhibit significant degradation. A mass of extracellular matrix and fibrous tissue were distributed around the implanted films, and a few neutrophils were observed in the fibrous tissue. In addition, some new blood vessels were formed around the implanted films. These results indicated that all of experimental films owned good biocompatibility *in vivo*.

Osteogenic differentiation of MSCs on various films in vivo

To explore whether the SF, A-SF, SF-nHAp and A-SF-nHAp films could induce the bone-like tissue formation in vivo, these films seeded with MSCs were subcutaneously implanted into the back of SD rats, followed by immumohistochemical staining of the osteogenic marker proteins (Fig. 7), including osteopontin (OPN), osteocalcin (OCN) and type I collagen (Col- I). According to the semi-quantitative result of immumohistochemical staining, more Col- I was deposited around the A-SF (AOD = 0.46 ± 0.02) and A-SF-nHAp (AOD = 0.47 ± 0.01) groups than around the SF (AOD = 0.42 ± 0.009) and SF-nHAp (AOD = 0.41 ± 0.01) groups ($P < 0.01$). But the Col- I expression did not present difference between A-SF and A-SF-nHAp group. SF and SF-nHAp group also did not show the difference for the Col- I expression. On the other hand, Col- I was more organized around the A-SF and A-SF-nHAp films than around the SF and SF-nHAp films. OCN staining displayed the positive expression in the A-SF and A-SF-nHAp groups whereas OPN staining only showed the positive expression in the A-SF-nHAp group. Besides, more OCN was deposited on A-SF-nHAp group (AOD = 0.36 ± 0.006) than A-SF group (AOD = 0.32 ± 0.008) ($P < 0.05$). These results suggested that the osteogenesis induced by the A-SF and A-SF-nHAp films was more efficient than that by the SF and SF-nHAp films. Furthermore, more bone-like tissue was deposited on the mineralized A-SF films than on the non-mineralized counterparts, but no significant difference between SF and SF-nHAp was found. These results collectively show that a combination of the plasma treatment and the subsequent mineralization significantly improved the in vivo osteogenesis induction capability of the SF films.

Discussion

Plasma treatment was a classical method for modifying surfaces and usually employed to improve the properties of substrate surfaces, such as roughness and hydrophilicity. During the plasma treatment, a partially ionized gas, including excited molecules, cations, anions, radicals, electrons, and atoms, etc, interacted with the surface of substrates.[30] In this study, the topographical changes of the SF surface (from smooth to nano-pillared) as characterized by SEM (Fig. 2A) were attributed to the etching by the ionized gas. Also, the intensity of amide-specific peaks in the FT-IR spectra was lower for A-SF than for the pristine SF (Fig. 4A), probably resulting from the breaking of the amide V and amide I groups under the bombing of the ionized gas.[31] Besides, some C-C and C-H bonds were broken due to the air plasma treatment. As a consequence, some active chemical groups (such as -CH2•, -NH•) emerged and reacted with oxygen in air, resulting in the increase of oxygen-containing polar functional groups (Fig. 4C).[19, 31, 32] Furthermore, the incorporation of polar groups into the

films due to the reaction of O led to the improvement of hyprophilicity of the SF surface after air-plasma treatment (Fig. 3b), as verified by the contact angle measurement. Crystalline regions of the SF molecules could be partially decomposed or oxidized with the radiation of air plasma, which was confirmed by the XRD result where the amount of random roils was increased (Fig. 4B). Therefore, air plasma treatment allowed us to successfully prepare SF films with a unique nano-pillar topography and good hydrophilicity.

Surface topography can direct the differentiation of MSCs.[33] Various substrates with different kinds of nano- and micro-topography were demonstrated to directly induce the differentiation of MSCs, such as protein nanoridges,[23] nHAp,[34] etc. In this study, MSCs on the A-SF films with nano-pillars showed more efficient osteogenesis than those on the SF films. In comparison with the pristine SF films, the A-SF films owned more oxygen, and thus were more hydrophilic and displayed unique (nano-pillared) nanotopography. Though the hydrophilicity could control the differentiation of MSCs through influencing the adhesion and spreading of MSCs,[35] the difference in the hydrophilicity between the surface of the SF and A-SF films was not remarkable enough to affect the MSCs adhesion and spreading according to the observation of the morphology and early proliferation of the MSCs in this study (Fig. 5). Conversely, nanotopography could regulate the differentiation of MSCs not only via impacting the adhesion and spreading of MSCs but also through the local mechanical stimulation. Hence, for the non-mineralized SF films, we believed that the nano-pillars on the A-SF surface produced by air-plasma treatment promoted the osteogeneic differentiation of MSCs, rather than the hydrophilicity.

To introduce the bone component, nHAp, onto bone regenerative biomolecular materials, the biomolecular materials were used as a template to form HAp.[36, 37] In this study, needle-like and plate-like nHAp were mineralized on the SF and A-SF films, respectively. Besides, the plate-like nHAp crystals on the A-SF films exhibited a higher crystallinity than the needle-like nHAp crystals on the SF films. In general, the surface properties, such as the topography, roughness, hydrophilic-hydrophobic property, charge, etc., can influence the mineralization of nHAp on various surfaces. The A-SF surface with unique nano-pillared topography and higher hydrophilicity induced the formation of bone-like plate-shaped nHAp of increased crystallinity when compared to the pristine SF surface. The plate-shaped nHAp is more similar to the natrual plate-lilke HAp in compact bone in terms of morphology[38–40] and may show a better ability to promote the osteogenesis (Fig. 7).

Indeed, for the mineralized SF films, MSCs on the A-SF-nHAp exhibited more efficient bone formation than those on the SF-nHAp (Fig. 7). According to the characterization of static contact-angle, XPS and FT-IR, no difference in the hydrophilicity and compositions was found between the two mineralized films. The difference in the nanotopography and crystallinity of the nHAp on the surface of the two mineralized films was the only factor that could induce the difference in the osteogenesis between the two substrates. In this study, the air-plasma treatment changed the content of oxygen, hydrophilicity,[41] and topography[42] of the surface of the SF films, which in turn influenced the nucleation and crystallizaiton of nHAp during the mineralization. This is the possible reason why the SF and A-SF films induced the formation of nHAp of different shapes and crystallinity.

Conclusions

Plate-shaped and needle-like nHAp were first synthesized on the SF films with and without modification by air-plasma treatment, respectively. The air-plasma treatment for only 5 min allowed the SF films to become more hydrophilic and bear nano-pillars, enabling the resultant films to template the formation of bone-like plate-shaped crystalline nHAp. Four groups of SF films seeded with MSCs were compared in terms of in vivo osteogenesis in a subcutaneous rat model, including pristine SF films (SF), nHAP-mineralized SF films (SF-nHAp), air-plasma-treated SF films (A-SF), and nHAP-mineralized A-SF films (A-SF-nHAp). It was discovered that the A-SF-nHAp and A-SF films more efficiently promoted the formation of bone-like tissue than the SF and SF-nHAp films. Moreover, the A-SF-nHAp films were more efficient in promoting bone formation than the A-SF films whereas the SF and SF-nHAp films did not show obvious difference in promoting bone formation. Namely, a combination of the air-plasma treatment and the subsequent nHAp mineralization most efficiently promoted the formation of bone-like tissue. This work manifests that a scaffold with plate-shaped nHAp decorating the air-plasma-treated SF matrix is a good candidate for bone regeneration. The air-plasma treatment is a low-temperature physical method that does not use reagents other than the air and usually does not cause chemical damage on the protein-based biomaterials. Thus our plasma-based method is an attractive new route for surface modification of silk protein based biomaterials for enhanced tissue regeneration.

Acknowledgements

The authors acknowledge the support of Zhejiang Provincial Natural Science Foundation of China (LZ17C170002 and LZ16E030001), National Natural Science Foundation of China (51673168, 81871499, and 31800807), State of Sericulture Industry Technology System (CARS-18-ZJ0501), Zhejiang Provincial Science and Technology Plans (2016C02054-19), the Fundamental Research Funds for the Central Universities (2018XZZX001-11), the National Key Research and Development Program of China (2016YFA0100900), and China Postdoctoral Science Foundation (2018M630678). Y.J.S. and C.B.M. would also like to thank the financial support from National Institutes of Health (EB021339).

Notes and references

1. Lin KF, He S, Song Y, Wang CM, Gao Y, Li JQ, Tang P, Wang Z, Bi L and Pei GX, Acs Appl Mater Interfaces, 2016, 8, 6905–6916. [PubMed: 26930140]
2. Wagener V, Boccaccini AR and Virtanen S, Applied Surface Science, 2017, 416.
3. Cardoso GBC, Maniglio D, Volpato FZ, Tondon A, Migliaresi C, Kaunas RR and Zavaglia CAC, J Biomed Mater Res B Appl Biomater, 2016, 104, 1076–1082. [PubMed: 26033969]
4. Gogoi D, Choudhury AJ, Chutia J, Pal AR, Khan M, Choudhury M, Pathak P, Das G and Patil DS, Biopolymers, 2014, 101, 355–365. [PubMed: 23913788]
5. Yang M, He W, Shuai Y, Min S and Zhu L, Journal of Polymer Science Part B Polymer Physics, 2013, 51, 742–748.
6. Yang M, Shuai Y, Zhang C, Chen Y, Zhu L, Mao C and OuYang H, Biomacromolecules, 2014, 15, 1185–1193. [PubMed: 24666022]
7. Jiang J, Hao W, Li Y, Yao J, Shao Z, Li H, Yang J and Chen S, Biotechnology Letters, 2013, 35, 1349–1350.
8. Liu H, Xu GW, Wang YF, Zhao HS, Xiong S, Wu Y, Heng BC, An CR, Zhu GH and Xie DH, Biomaterials, 2015, 49, 103–112. [PubMed: 25725559]
9. Xie J, Peng C, Zhao Q, Wang X, Yuan H, Yang L, Li K, Lou X and Zhang Y, Acta Biomaterialia, 2016, 29, 365–379. [PubMed: 26441129]

10. Chen W, Xu K, Tao B, Dai L, Yu Y, Mu C, Shen X, Hu Y, He Y and Cai K, Acta Biomaterialia, 2018, 74, 489–504. [PubMed: 29702291]
11. Morin EA, Tang S, Rogers KL and Wei H, Acs Appl Mater Interfaces, 2016, 8, 5737–5745. [PubMed: 26881298]
12. Gonzalez Garcia LE, MacGregor-Ramiasa M, Visalakshan RM and Vasilev K, Langmuir, 2017, 33, 7322–7331. [PubMed: 28658956]
13. Chen Z, Bachhuka A, Han S, Wei F, Lu S, Visalakshan RM, Vasilev K and Xiao Y, ACS Nano, 2017, 11, 4494–4506. [PubMed: 28414902]
14. Murphy AR and Kaplan DL, Journal of Materials Chemistry, 2009, 19, 6443–6450. [PubMed: 20161439]
15. Meng C, Chen Y, Xie M, Yu Z and Yang B, Journal of Biomedical Materials Research Part A, 2018, 106, 321–332. [PubMed: 28921868]
16. Petlin DG, Tverdokhlebov SI and Anissimov YG, Journal of Controlled Release, 2017, 266, 57–74. [PubMed: 28935595]
17. Amornsudthiwat P, Mongkolnavin R, Kanokpanont S, Panpranot J, Wong CS and Damrongsakkul S, Colloids & Surfaces B Biointerfaces, 2013, 111, 579–586. [PubMed: 23893032]
18. Cheon YW, Lee WJ, Baek HS, Lee YD, Park J-C, Park YH, Ki CS, Chung K-H and Rah DK, Artificial Organs, 2010, 34, 384–392. [PubMed: 20633153]
19. Iriyama Y, Journal of Photopolymer Science & Technology, 2003, 16, 75–80.
20. Lee M, Ko Y-G, Lee JB, Park WH, Cho D and Kwon OH, Macromolecular Research, 2014, 22, 746–752.
21. Wang J, Yang S, Li C, Miao Y, Zhu L, Mao C and Yang M, ACS Applied Materials & Interfaces, 2017, 9, 22259–22267. [PubMed: 28665103]
22. Wang X, Zhuang J, Peng Q and Li YD, Advanced Materials, 2006, 18, 2031–2034.
23. Yang M, Shuai Y, Sunderland KS and Mao C, Advanced Functional Materials, 2017, 27, 1703726. [PubMed: 29657571]
24. Zheng C, Chen G and Qi Z, Plasma Chemistry and Plasma Processing, 2012, 32, 629–642.
25. Lu YH, Lin H, Chen YY, Wang C and Hua YR, Fibers and Polymers, 2007, 8, 1–6.
26. Yan LP, Salgado AJ, Oliveira JM, Oliveira AL and Rui LR, Journal of Bioactive & Compatible Polymers, 2013, 28, 439–452.
27. Jin Y, Kundu B, Cai Y, Kundu SC and Yao J, Colloids & Surfaces B Biointerfaces, 2015, 134, 339–345. [PubMed: 26209967]
28. Anwar A, Asghar MN, Kanwal Q, Kazmi M and Sadiqa A, Journal of Molecular Structure, 2016, 1117, 283–286.
29. Goloshchapov DL, Gushchin MS, Kashkarov VM, Seredin PV, Ippolitov YA, Khmelevsky NO and Aksenenko AY, Results in Physics, 2018.
30. Kuriakose S, Ahmed T, Balendhran S, Collis GE, Bansal V, Aharonovich I, Sriram S, Bhaskaran M and Walia S, Applied Materials Today, 2018, 12, 244–249.
31. Gogoi D, Choudhury AJ, Chutia J, Pal AR, Dass NN, Devi D and Patil DS, Applied Surface Science, 2011, 258, 126–135.
32. Kim KS, Chang MR, Chan SP, Sur GS and Chan EP, Polymer, 2003, 44, 6287–6295.
33. Dalby MJ, Gadegaard N, Tare R, Andar A, Riehle MO, Herzyk P, Wilkinson CD and Oreffo RO, Nature Materials, 2007, 6, 997–1003. [PubMed: 17891143]
34. Zhao C, Wang X, Gao L, Jing L, Zhou Q and Chang J, Acta Biomaterialia, 2018, 73, 509–521. [PubMed: 29678674]
35. Hao L, Yang H, Du C, Fu X, Zhao N, Xu S, Cui F, Mao C and Wang Y, Journal of Materials Chemistry B, 2014, 2, 4794–4801. [PubMed: 25328680]
36. Siqueira IAWB, Corat MAF, Cavalcanti B. d. N., Neto WAR, Martin AA, Bretas RES, Marciano FR and Lobo AO, ACS Applied Materials & Interfaces, 2015, 7, 9385–9398. [PubMed: 25899398]
37. Xiao Z, Que K, Wang H, An R, Chen Z, Qiu Z, Lin M, Song J, Yang J and Lu D, Dental Materials Official Publication of the Academy of Dental Materials, 2017, 33, 1217. [PubMed: 28774431]

38. Daculsi G and Kerebel B, Journal of Ultrastructure Research, 1978, 65, 163–172. [PubMed: 731784]
39. Raspanti M, Guizzardi S, Pasquale VD, Martini D and Ruggeri A, Biomaterials, 1994, 15, 433–437. [PubMed: 8080934]
40. Zhuang Z, Yoshimura H and Aizawa M, Materials Science and Engineering: C, 2013, 33, 2534–2540. [PubMed: 23623065]
41. Hartgerink JD, Beniash E and Stupp SI, Science, 2001, 294, 1684–1688. [PubMed: 11721046]
42. Pisarek M, Roguska A, Andrzejczuk M, Marcon L, Szunerits S, Lewandowska M and Janik-Czachor M, Applied Surface Science, 2011, 257, 8196–8204.

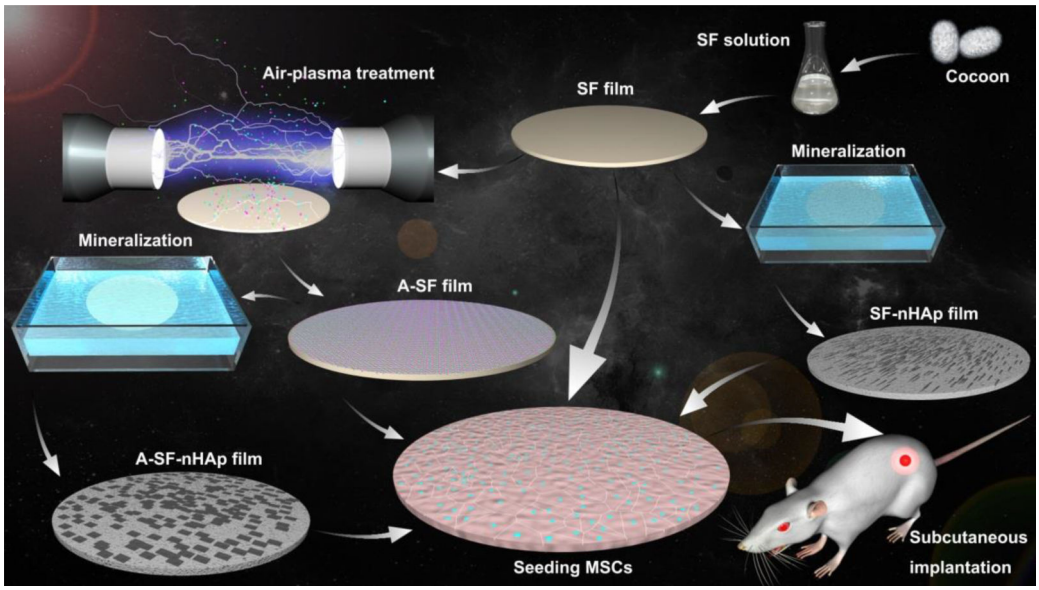

Fig. 1.

Schematic illustration of the preparation, air-plasma treatment and mineralization of silk fibroin (SF) films as well as their use in inducing bone formation in vivo in a rat subcutaneous model. SF solution extracted from cocoon was fabricated into SF films by casting and soaking into a 70% (v/v) methanol solution. The SF films were treated with air-plasma for 5 min to become A-SF films. Both SF and A-SF films were futher mineralized to form needle-like and plate-like nano-hydroxyapatite (nHAp) on them, producing composite films termed SF-nHAp and A-SF-nHAp, respectively. The four films, SF, A-SF, SF-nHAp and A-SF-nHAp, were seeded with mesenchymal stem cells (MSCs) and then subcutaneously implanted into the back of the rats. The A-SF-nHAP films promoted the ectopic bone formation most efficiently among all of the four groups.

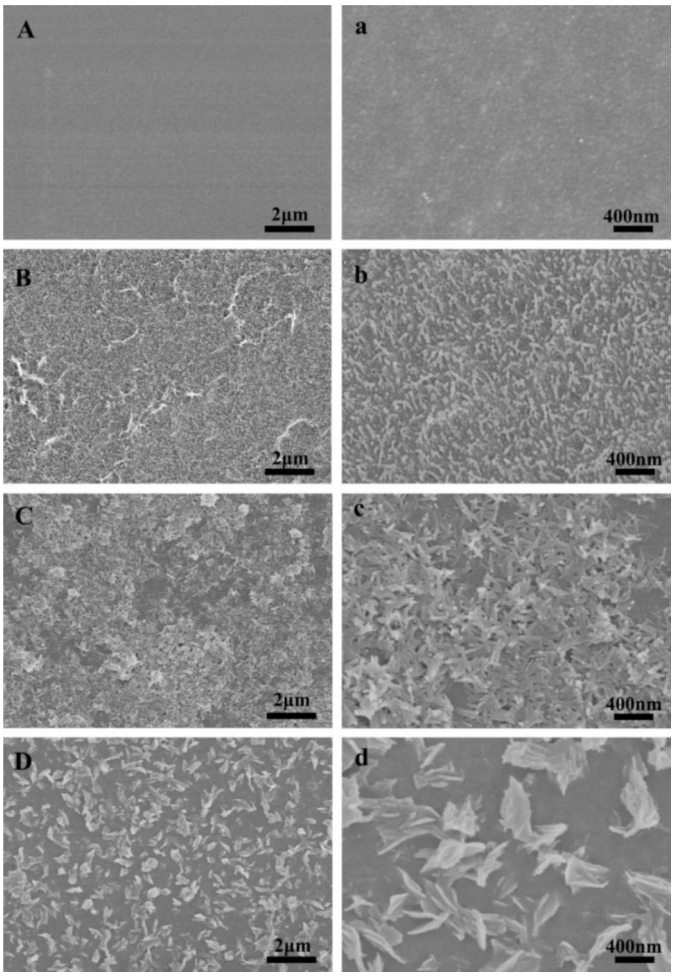

Fig. 2.

Morphological characterization of silk fibroin (SF) films after different treatments by SEM. (A, a) The pristine SF film. (B, b) Air-plasma-treated SF film (A-SF). (C, c) Mineralized pristine SF films (SF-nHAp). (D, d) Mineralized A-SF film (A-SF-nHAp). a, b, c and d are the high magnification images of A, B, C and D, respectively. Nano-pillars were observed on the surface of the A-SF films. Nano-needle-like and nano-plate-like hydroxyapatite were uniformly distributed on the SF-nHAp and A-SF-nHAp films, respectively.

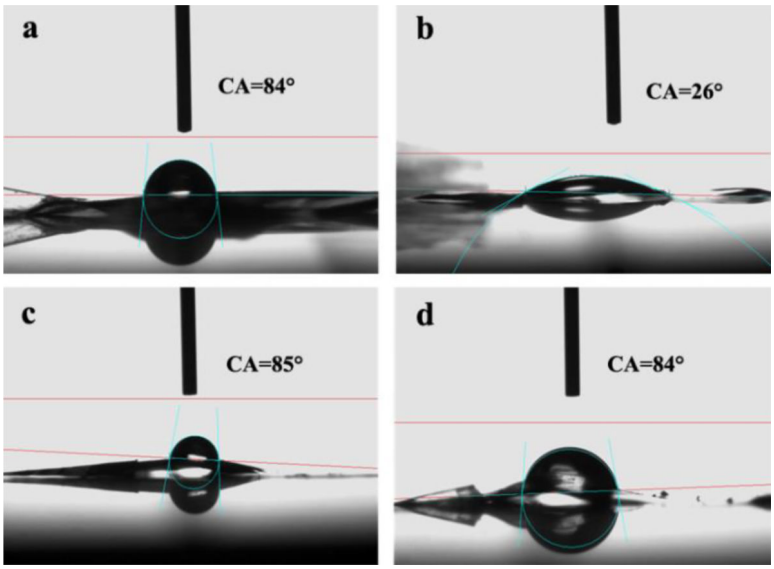

Fig. 3.

Hydrophilicity of the SF films reflected by water static contact angle measurement. (a, c) Pristine SF film before (a) and after (c) mineralization. (b, d) Air-plasma-treated SF (A-SF) film before (b) and after (d) mineralization. The surface of air-plasma treated SF films was more hydrophilic than the other films.

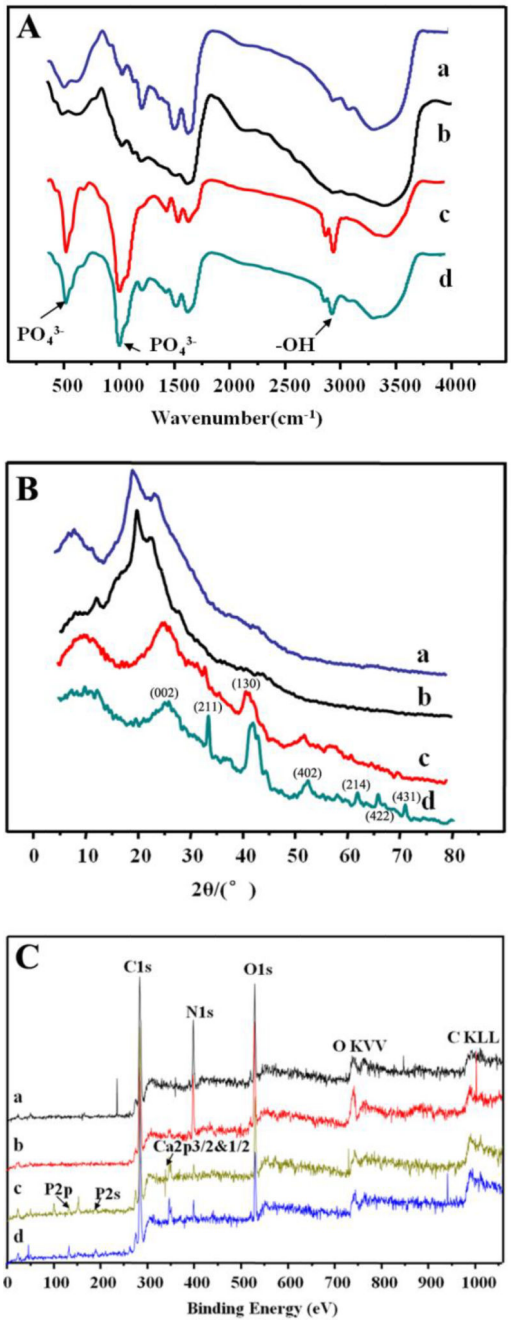

Fig. 4.

Structural characterization of the SF films after different treatments by FT-IR (A), XRD (B) and XPS (C). a and c are the pristine SF film before (a) and after (c) mineralization. b and d are the A-SF film before (b) and after (d) mineralization. The surface of A-SF films owned more oxygen content and random coils. The nHAp formed on the A-SF films showed a higher crystalline degree than that on the pristine SF films. The indexed peaks in B were corresponding to HAp structure.

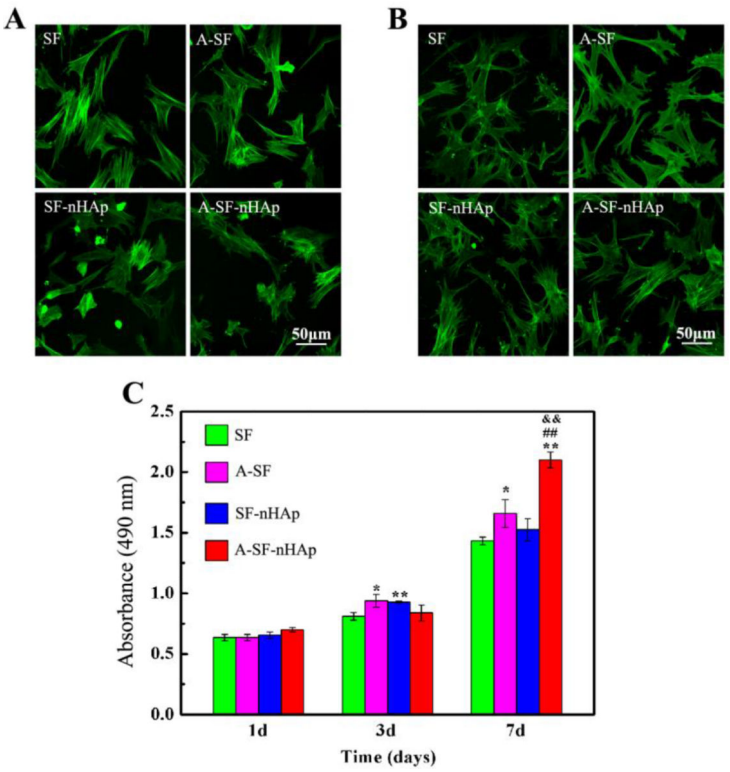

Fig. 5.

Morphologies and proliferation of MSCs after seeded on differently treated SF films. (A, B) The morphology of MSCs characterized by actin staining after being seeded for 1 day (A) and 3 days (B). (C) The proliferation of MSCs revealed by Cell Proliferation Assay Kit. (*) $p < 0.05$ and (**) $p < 0.01$ vs SF group; (##) $p < 0.01$ vs A-SF group; (&&) $p < 0.01$ vs SF-nHAp group. MSCs owned more pseudopods on the A-SF, SF-nHAp and A-SF-nHAp than those on the SF surface on day 3. MSCs on the A-SF and A-SF-nHAp showed stronger proliferation ability than those on the SF and SF-nHAp. SF: pristine SF film; A-SF: air-plasma-treated SF film; SF-nHAp: SF film with mineralized nHAp; A-SF-nHAp: A-SF film with mineralized nHAp.

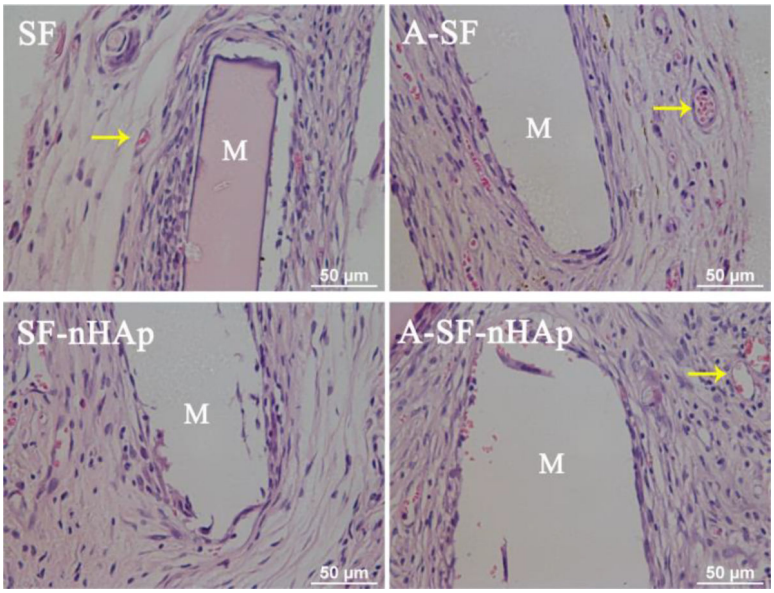

Fig. 6.

H&E staining of SF, A-SF, SF-nHAp and A-SF-nHAp films seeded with MSCs in subcutaneously implanted rat model after 4 weeks. Yellow arrows indicated the new vessels. Well-organized MSCs, a small number of neutrophils and some new vessels were observed around all films, suggesting a mild inflammatory response and good biocompatibility of SF, SF-nHAp, A-SF and A-SF-nHAp films. SF: pristine SF film; A-SF: air-plasma-treated SF film; SF-nHAp: SF film with mineralized nHAp; A-SF-nHAp: A-SF film with mineralized nHAp; M: implanted materials.

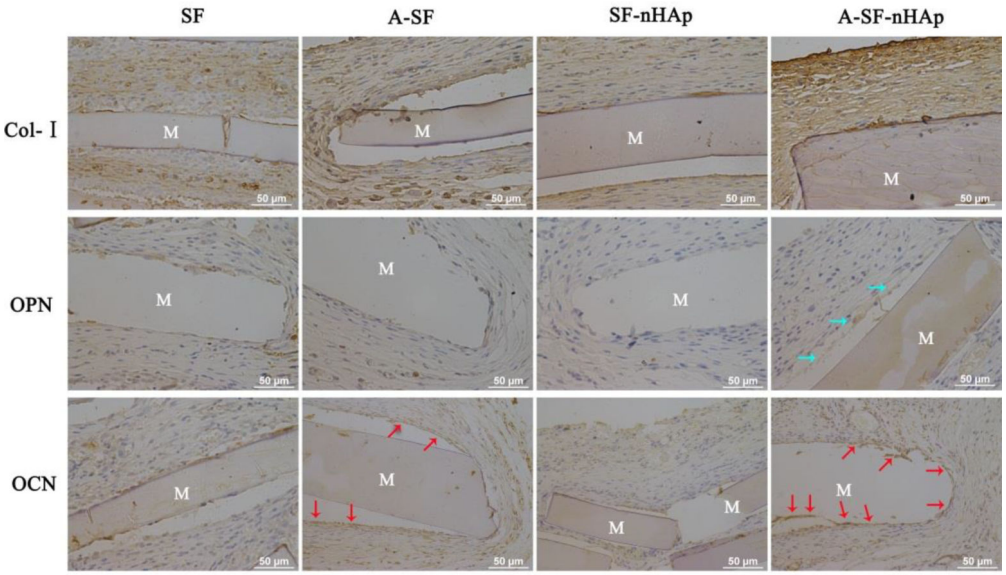

Fig. 7.

In vivo osteogenesis induced by differently treated SF films. Immunohistochemical staining of Col I, OPN and OCN in the subcutaneously implanted SF, A-SF, SF-nHAp and A-SF-nHAp films seeded with MSCs. Blue and red arrows indicated the positive expression of OPN and OCN, respectively. Immunohistochemical staining showed that more bone matrix proteins were deposited around the A-SF and A-SF-nHAp films than around the SF and SF-HAp films. Moreover, more OPN was deposited around the A-SF-nHAp than around A-SF films. SF: pristine SF film; A-SF: air-plasma-treated SF film; SF-nHAp: SF film with mineralized nHAp; A-SF-nHAp: A-SF film with mineralized nHAp; M: implanted materials.